

PCCP

Accepted Manuscript



This is an *Accepted Manuscript*, which has been through the Royal Society of Chemistry peer review process and has been accepted for publication.

Accepted Manuscripts are published online shortly after acceptance, before technical editing, formatting and proof reading. Using this free service, authors can make their results available to the community, in citable form, before we publish the edited article. We will replace this *Accepted Manuscript* with the edited and formatted *Advance Article* as soon as it is available.

You can find more information about *Accepted Manuscripts* in the [Information for Authors](#).

Please note that technical editing may introduce minor changes to the text and/or graphics, which may alter content. The journal's standard [Terms & Conditions](#) and the [Ethical guidelines](#) still apply. In no event shall the Royal Society of Chemistry be held responsible for any errors or omissions in this *Accepted Manuscript* or any consequences arising from the use of any information it contains.

Ab Initio Study of the Influence of Resonance Stabilization on Intramolecular Ring Closure Reactions of Hydrocarbon Radicals

Kun Wang, Stephanie M. Villano, and Anthony M. Dean*

Chemical and Biological Engineering Dept., Colorado School of Mines, Golden, CO 80401

*corresponding author: amdean@mines.edu, (303) 273-3643

Abstract

The intramolecular ring closure reactions of unsaturated hydrocarbon radicals potentially play an important role for the formation of molecular weight growth species, especially during the pyrolysis and oxidation of alkenes under low to intermediate temperatures. In this work we investigated a series of intramolecular cycloaddition reactions of both allylic- and alkyl-type dienyl radicals. In the first set of reactions, a resonant linear radical is converted into a non-resonant cyclic radical. In the second set, a non-resonant linear alkenyl radical isomerizes to either a resonant cyclic radical or a cyclic carbinyl radical. In both cases, three different reaction schemes are examined based on the location of the partially-formed resonance structure in the cyclic transition state. For each reaction scheme, both the endo- and exo-pathways were investigated. High pressure rate parameters are obtained from the results of CBS-QB3 electronic structure calculations combined with canonical transition state theory calculations. The results are discussed in the context of a Benson-type model to examine the impact of the partially-formed resonance stabilization on both the activation energies and pre-exponential factors. The results are compared to previously reported rate parameters for cycloaddition reactions of alkenyl radicals. The differences in the activation energies are primarily due to the bimolecular component of the activation energy. However, in some cases, the presence of the partial resonance structure significantly increases the strain energy for the ring that is formed in the transition state. The pre-exponential factors are also impacted by the formation of a partial resonance structure in the transition state. Lastly, the C_6H_9 potential energy surface is examined to show how the trends that are outlined here can be used to estimate rate parameters, which are needed to analyze pressure-dependent reaction systems.

Key words: intramolecular ring closure reactions, addition reactions, Benson-type model, rate estimation rules

Introduction

A particular challenge in many hydrocarbon energy conversion processes is the formation of molecular weight growth species. The formation of these species is problematic since they can lead to the formation of deposits or soot, which reduces the application's efficiency and limits the run times between decoking operations and/or catalyst regeneration cycles. The presence of molecular weight growth species in exhaust gas emissions is also an environmental and health problem. In spite of much research on these reactions, uncertainties remain.^{1, 2} For these reasons, more research is needed to better characterize the hydrocarbon pyrolysis reactions that are responsible for much of the undesired molecular weight growth chemistry. Further, it is useful to be able to express the rate coefficients for these reactions in the form of rate estimation rules so that they can be applied to detailed kinetic modeling efforts. These models can be used to identify the experimental conditions that might minimize this undesirable chemistry.

One important reaction class that provides a low energy route to the formation of molecular weight growth products are intramolecular ring closure reactions (also called cycloaddition or cyclization reactions). To illustrate this, consider the cycloaddition reaction of 1-pent-4-enyl radical ($C=CCCC^{\bullet}$),³ which can be formed from the addition reaction of allyl plus ethylene. A simplified version of the C_5H_9 potential energy surface shown in Figure 1. Once formed, it is energetically more favorable for the 1-pent-4-enyl adduct (species 1) to cyclize than it is to dissociate back to the reactants (I) via the β -scission reaction; the other reaction channels (e.g., 1 to 2, 3, and V) also have much higher energy barriers. Cycloaddition can occur via two routes. Addition to the near vinylic carbon (the 2-position) leads to a cyclobutyl-carbinyl radical (4); this is referred to as an exo-cycloaddition. Addition to the far vinylic carbon (the 1-position) leads to cyclopentyl radical (5); this is referred to as an endo-cycloaddition. The barriers for the two cycloaddition channels are comparable for this case. However, once formed, the cyclobutyl-carbinyl radical (4) is more likely to ring-open back to the 1-pent-4-enyl radical (1) than it is to β -scission to form methylene-cyclobutane plus H (VI). In contrast, the β -scission barrier for cyclopentyl radical (5) to form cyclopentene plus H (II) is comparable to that for ring opening to (1). Subsequent reactions of cyclopentene can lead to cyclo-1,3-pentadiene,⁴⁻⁶ which is known to be an important intermediate in formation of larger molecular weight growth species.⁷⁻¹¹

Due to their importance, several prior experimental and theoretical studies have investigated the cycloaddition reactions of alkenyl radicals or their reverse ring opening reactions.¹²⁻²² Recently, we developed a series of high-pressure rate rules for both the exo- and endo-cycloadditions of alkenyl radicals based on CBS-QB3 electronic structure calculation coupled with transition state theory calculations.²³ The results show that, over a restricted temperature range, the rate parameters can be formulated using a Benson-type structure-reactivity relationship.²⁴ This type of relationship provides a physical framework for which to interpret rate parameters assignments. The activation energies are considered to consist of two

parts: the activation energy of the corresponding bimolecular addition reaction plus the ring strain energy ($E_a = E_{bi} + E_{RS}$). The pre-exponential factors are calculated from the entropy difference between the reactant and transition state, and this difference correlates with the loss of internal rotors in the cyclic transition state structure. Consistent with several previous studies,^{12, 13, 18, 19, 25, 26} the results show that the exo-cycloaddition pathways are generally favored over the endo-pathways, even for cases where the formation of the endo-products are favored thermodynamically. This is due to the higher pre-exponential factor and lower ring strain energy. However, as shown above for the cyclization of the 1-pent-4-enyl radical, the endo-pathway still may be dominant since the subsequent β -scission reaction of the cycloalkyl radical is favorable.

This type reaction is especially important for describing the molecular weight growth formation in the olefin pyrolysis, where the addition of resonantly-stabilized radicals to the dienes play significant roles.³ Yet there is very limited work investigating the influence of resonance stabilization on these reactions. In this work we investigate the impact of resonance stabilization on this reaction class by examining the cycloaddition reactions of a series of dienyl radicals. These radicals can be formed from H-atom abstraction from dienes either at an allylic site or an alkyl site. For the allylic-type radicals, cycloaddition converts a resonantly stabilized radical into a non-stabilized cyclic radical. This conversion can occur via three distinct cases (shown in schemes 1-3 in Table 1), depending on the location of the partially-formed resonance structure in the transition state. In scheme 1 the reaction proceeds through a transition state ring where only one of the three carbon atoms in the partially-formed allylic structure is contained in the ring, with the other two are located outside of the ring. In scheme 2, two of the carbon atoms in the partially-formed allylic structure are located in the transition state ring, with the third one is outside of the ring. In scheme 3 the partially-formed allylic structure is completely contained inside of the transition state ring. For the alkyl-type dienyl radicals, cycloaddition via the endo-pathway converts a non-stabilized radical into a resonantly stabilized cyclic radical. The exo-pathway forms a non-stabilized cyclic carbinyl radical. For these reactions, three types of transformations are also investigated. These are shown by the reactions in schemes 4-6 in Table 1. Similar to the above three schemes, schemes 4-6 have 1, 2, and 3 carbon atoms, respectively, in the partially-formed resonance structure within the transition state ring.

The presence of resonance stabilization in the reactant and/or product may significantly impact the activation energy, both in terms of the bimolecular and ring strain components, as well as the pre-exponential factors. This has previously been observed for intramolecular H-atom shift reactions of hydrocarbon radicals, which also proceed via cyclic transition state.²⁷ The bimolecular component of the barrier for the reactions in schemes 1-3 can be estimated from that for allylic radical addition an olefin. Because the reactant radical is resonantly stabilized, the barrier for allylic radical addition is greater than that for the corresponding alkyl radical addition.^{3, 28, 29} For schemes 4-6, the bimolecular component of the barrier can be estimated from the addition reaction of an alkyl radical to a diene; the activation energy for addition to a

conjugated diene, forming a resonantly-stabilized radical, is lower than the addition to regular olefins.³ Depending upon the location of the resonance structure in the transition state structure, the ring strain component may also vary due to structural restrictions. The presence of the partial resonance structure in the transition state ring will also impact the pre-exponential factors. For example, the presence of partial resonance may restrict some of the hindered rotors or increase the rigidity of the ring.

The aim of this work is to explore how resonance stabilization influences the rate parameters for this reaction class and to generalize the results so that they can be applied in kinetic modeling efforts. Specifically, we investigate the series of cycloaddition reactions of both allylic- and alkyl-type dienyl radicals shown in schemes 1-3 and 4-6, respectively. For each reaction scheme, the size of the ring in the transition state is systematically increased to a 7-membered ring for the endo-pathway and a 6-membered ring for the exo-pathway. In addition to these sets of reaction, we also investigate the cycloaddition reaction of allyl radical as well as a few select cases where there is extended resonance. High pressure rate constants are obtained from the results of CBS-QB3 electronic structure calculations combined with canonical transition state theory calculations over the temperature range of 300-2500 K and the results are presented in modified Arrhenius form. The results are also presented in the context of the Benson-type model over a narrower temperature range. The results are compared to those of prior studies involving dienyl radicals,^{19, 30} and the impact of resonance stabilization on activation energies and pre-exponential factors are examined and compared to those of alkenyl radical reactions.²² Lastly, we examine the C₆H₉ potential energy surface to illustrate the importance of these pathways and to show how the trends that are outlined here can be used to estimate rate parameters, which are needed to analyze pressure-dependent reaction systems.

Methods

Electronic structure calculations in this research were carried out using the Gaussian 03 and 09 suites of programs.^{31, 32} The CBS-QB3 composite method³³ was used to calculate optimized geometries, frequencies, and electronic energies for the lowest energy conformer of the reactants, products, and transition states. This method has been shown to predict heats of formation for a large test set of molecules with an accuracy of just over 1 kcal/mol.³³ Low frequency vibrational modes that resemble torsions around single bonds were treated as hindered internal rotors rather than as harmonic oscillators. Hindrance potentials were calculated at the B3LYP/6-31G(d) level of theory via relaxed surface scans with a step size of 10 degrees. Hindered potentials (with barriers \leq 12 kcal/mol) were fitted to truncated Fourier series expansions. Reduced moments of inertia for asymmetric internal rotors were calculated at the I(2,3) level based on the equilibrium geometry as defined by East and Radom.³⁴ The 1-D Schrödinger equation was numerically solved for each internal rotor using the eigenfunctions of the 1-D free rotor as basis functions. The energy eigenvalues are then used to numerically

calculate their contributions to thermodynamic functions. All other modes were treated as harmonic oscillators and the frequencies were scaled by a factor of 0.99. Thermodynamic properties (e.g., $\Delta_f H_{298}$, S_{298} , and C_p values) were calculated using standard statistical mechanics methods. The electronic energy of each species was converted to its heat of formation using the atomization method. Since only relative energies are required in this work, no attempts were made to improve the heats of formation using, for example, bond additivity corrections. Inspections of the hindered rotor potentials help ensure that the optimized geometry of a molecule corresponds to the lowest energy minimum. A normal mode analysis was performed to identify the nature of the species. Transition states were identified by having one imaginary frequency, which was animated to verify that it corresponds to the desired reaction coordinate.

High-pressure rate coefficients were calculated using canonical transition state theory (TST): $k(T) = \kappa(T) \cdot k_B T/h \cdot \exp(-\Delta G^\ddagger/RT)$, where $\kappa(T)$ is the tunneling correction factor, and ΔG^\ddagger is the Gibbs free energy difference between the transition state, minus the contribution from the reaction coordinate, and the reactants. The remaining variables have their usual meaning. Tunneling correction factors were calculated with an asymmetric Eckart potential.³⁵ Rate constants were calculated over a temperature range of 300 – 2500 K in 50 K increments and fit to modified Arrhenius expressions: $k(T) = A' \cdot T^n \cdot \exp(-E/RT)$. Simple Arrhenius fits were obtained over the limited temperature range of 500 – 1500 K and at 298K as well to facilitate analysis using the Benson model. The simple Arrhenius parameters are determined from $E_a = E + nRT$ and $A = k(T)/\exp(-(E + nRT)/RT)$, where the “n” and “E” parameters are taken from the modified Arrhenius fits. The error in the pre-exponential factor is on the order of a factor of 2 at 1000K. While some error from the hindered rotor treatment cancels on the TST rate constant formula, if the number of rotors on the reactants and transition state are significantly different, the uncertainty will be larger. The error in the activation energy is estimated to be ~1 kcal/mol. Together, this leads to an uncertainty of a factor of ~3 at 1000 K in the calculated rate coefficients. Uncertainties arise from errors in the *ab initio* method such as variations in optimized reactant and transition state geometries as well as errors in the harmonic frequencies and hindered rotor calculations.

In several of the investigated reaction schemes, the allylic group is either fully or partially outside of the transition state ring. This leads to the presence of multiple isomers. Similarly, in some of the reactions, the transition state ring may contain alkyl substituents resulting in one or more isomers. For these cases, the rate constants for each isomer were summed at each temperature, and then fit in the whole range to obtain the Arrhenius parameters. For these transition state ring structures with optical isomers, the entropies are corrected by adding $R \cdot \ln(2)$. However, if two or more substituents are present at different locations on the ring or if the ring is non-planar, these isomers are energetically distinct. Both the axial and equatorial structures were calculated, leading to two or more rate constants, which were then summed to get a total value.

Lastly, we examine the C_6H_9 potential energy surface. The pressure- and temperature-dependent rate constants were calculated based on a steady state analysis in which the energy-dependent unimolecular rate coefficients, $k(E)$, were computed using Quantum-Rice-Ramsperger-Kassel (QRRK) theory. The density of states was calculated from three representative frequencies, which were extracted from heat capacities that were either obtained from the CBS-QB3 results or estimated from group additivity using THERM³⁶ or RMG.³⁷ The high-pressure rate constants are also used; these are either based on the CBS-QB3 results or they are estimated. Collisional stabilization rate constants were calculated using the modified strong collision (MSC)³⁸ assumption, and the average energy transferred per collision for the collider N_2 , $\langle \Delta E_{all} \rangle$, was -440 cal/mol. The Lennard-Jones collision diameters (σ_{LJ}) and well depths (ϵ_{LJ}) were estimated for adducts/isomers. More details of the methodology can be found in the work of Chang et al.,³⁹ and explicit comparisons of the results from this method to those from more rigorous approaches have also been provided in references.^{17, 40-45}

In several places throughout the text, tables, and figures, we employ a chemical notation that omits the hydrogen atoms. A radical site is indicated by a bullet, a double bond by an equal sign, and a conjugated bond by a dashed equal sign. For both endo- and exo-pathways, the following notation is used: For a 1,x-cycloaddition, x refers to the location of the carbon radical relative to the far vinylic carbon. For example, the reactions that are shown in Table 1 are 1,6-cycloadditions; the endo-pathway leads to a 6-membered ring radical, while the exo-pathway leads to a 5-membered ring radical. The units employed are kcal, sec, and mol.

Results and Discussion

Reactions of Resonant Linear Radicals

Tables 2-4 present the results for the endo- and exo-cycloaddition reactions of schemes 1-3, respectively. These reactions convert a resonantly-stabilized allylic linear radical into a non-allylic cyclic radical. In each case, the results for only the simplest reaction are included. For scheme 1, the investigated reactions include the 1,4 through the 1,7 endo- and exo-cycloadditions. For scheme 2, the 1,5 through the 1,7 reactions are investigated, while for scheme 3, the 1,6 and 1,7 reactions are investigated. For both the endo- and exo-reactions, the rate constants are fit over a temperature range of 300-2500 K to a modified Arrhenius form. The value “ n ” in the modified Arrhenius formula may be as high as ~ 1.5 , indicating that there is significant upward curvature on the Arrhenius plots. Thus, the use of the modified Arrhenius form is essential to properly describe the temperature dependence over a wide range. The rate constants are also fit to a simple Arrhenius form over a narrower temperature range (500-1500 K) or at a specific temperature (298 K). The ring strain energies (E_{strain}) for the various transition states are also provided. These values are calculated by subtracting the activation energies for corresponding bimolecular addition reactions from the overall activation energy. The reference bimolecular reactions correspond to allylic radical addition to olefins; these results are also obtained using

CBS-QB3 calculations and are provided in Table 5. Several additional reactions that follow schemes 1-3 are shown by Tables S1-S3 in the Supporting Information (SI).

For the endo-reactions in scheme 1 (Table 2), the activation energy decreases in going from a 4- to a 6-member transition state ring, and then slightly increases for the 7-member ring. For the exo-cycloaddition reactions, the 1,5 exo-reaction with 4-member transition state ring has the highest activation energies, followed by the 3-membered ring, while the larger transition state rings have the lowest barriers. The activation energies for the 1,5 through 1,7 endo- and exo-pathways are comparable. For the 1,4 cycloaddition reaction, the activation energy for the exo-pathway is significantly lower than the endo-pathway (~ 21 kcal/mol). The trends observed for the reactions in schemes 2 and 3 are similar. For scheme 2 (Table 3), the 1,6 endo- and exo-pathways with larger sized transition state rings have lower activation energies than the analogous 1,5 reactions. While the barrier of the 1,7 endo pathway is higher than the analogous 1,6 reaction, the barrier for the 1,7 exo-pathway is lower. In scheme 3 (Table 4), the activation energy increases in going from the 6- to a 7-member transition state ring for the endo-reactions; while it decreases in going from a 5- to a 6-membered ring transition state ring for the exo-reactions. These trends are similar to that observed for the alkenyl radical reactions forming saturated cyclic species.²³

The primary difference among the three different type of cycloaddition reactions in Tables 2-4 is the degree to which the partially-formed allylic group is incorporated into the transition state ring. For a given transition state ring size, the activation energies generally increase in going from scheme 1 to 2 to 3, reflecting the increasing amount of allylic conjugation formed in the transition state ring. The activation energies for the 1,5 endo- and exo-reactions in scheme 1 (i.e., reactions 1.2 and 1.6), with only one of the allylic carbon atoms in the ring, are ~ 4 and ~ 7 kcal/mol, respectively, lower in energy than the analogous reactions in scheme 2 (reactions 2.1 and 2.3), with two allylic carbons in the ring. The energy difference between the scheme 1 and 2 reactions become much smaller for the reactions that proceed through the larger sized transition state rings. The ring strain energies for the 1,6 endo- and exo-reactions in the scheme 2 (reactions 2.2 and 2.4) are ~ 8 and ~ 5 kcal/mol, respectively, lower than the corresponding reactions in scheme 3 (reactions 3.1 and 3.3), where the entire allylic structure is inside the transition state ring.

The analogous cycloaddition reactions of alkenyl radicals are used as reference reactions, in order to examine the impact of resonance structure on the various reaction schemes. Table 6 lists several calculated results for the 1,4 to 1,7 endo- and exo-reactions of alkenyl radicals.²² The comparison of activation energies for schemes 1-3 (as well as for schemes 4-6 that will be discussed later) to the alkenyl radical reactions is provided in the SI (Figure S1). The activation energies for scheme 1 are higher than those for the analogous alkenyl radical reactions, by about 6 to 7 kcal/mol at 298 K. The higher energy barriers is mostly due to the bimolecular component of energy barrier, which is ~ 5 kcal/mol higher for a resonantly-stabilized radical addition than it

is for an alkyl radical addition to a double bond. Compared to scheme 1, the activation energies for schemes 2 and 3 are much higher than those for the alkenyl radical reactions. For these two cases the differences are also due to the ring strain component of the activation energy. [Figure 2](#) shows the differences between the ring strain energies at 298 K for the reaction schemes 1-6 and the analogous alkenyl reactions. For the reactions in scheme 1, the ring strain energies are equal to or slightly larger than those for the corresponding alkenyl radical reactions; they are within 2-3 kcal/mol for either the endo- or exo-pathway. For the reactions in schemes 2 and 3, the differences are larger. The 1,6 endo-pathway in scheme 2 has a similar ring strain energy to that of the alkenyl reaction; while the 1,5 and 1,7 endo-reactions have 5 and 2.5 kcal/mol higher energy, respectively. The 1,5 through 1,7 exo-pathways are 9.7, 5, and 4 kcal/mol higher in energy, respectively, than the analogous alkenyl reactions. The ring strains for the scheme 3 reactions are 6-10 kcal/mol higher in energy for either endo- or exo-reactions. The CBS-QB3 optimized structures of the various transition states for schemes 1-6 as well as those from alkenyl reactions are provided in [Figures S2 and S3](#) in the SI. The bond lengths, bond angles, and distance between the two reacting carbon atoms in the transition states all together can be used to rationalize how the presence of the partially-formed allylic structure in the transition state impacts the ring strain energies.

For a given reaction scheme, the pre-exponential factors systematically decrease as the size of the transition state ring increases. This is because more entropy is lost in the formation of larger size transition state rings since a greater number of hindered rotors in the reactants are incorporated into the transition state ring. For a given reactant, the pre-exponential factor for the endo-pathway is smaller than that for the competing exo-pathway. This is because one more rotor is tied-up in the endo-transition state than in the exo-transition state. [Figure 3a and 3b](#) depicts the relationship between the pre-exponential factors and transition state ring sizes for schemes 1-3, as well as for the alkenyl radical reactions. The results from the [Tables S1-S3](#) are also incorporated in this figure. The pre-exponential factors for schemes 1-3 are consistently higher than those for the analogous alkenyl radical reactions. For scheme 3, this is consistent with the inclusion of the double bond in the transition state, which results in the loss of one less rotor.

For the endo-cycloaddition reactions of alkenyl radicals, the entropy loss can easily be determined on a per-rotor basis. However, for exo-cycloaddition pathway of alkenyl radicals and for both reaction pathways in schemes 1-3, it is difficult to simply count the number of rotors that are lost in the transition state. For example, for the exo-cycloaddition pathway in the alkenyl radical reactions, the C-C=C bending vibration is not constrained in the transition state, and this leads to an increased entropy (compared to the endo-transition state). To account for this, a gain of 0.5 rotor was assigned to allow the data for the exo-reactions to fall on the trend line for the endo-data.²³ For the reactions in schemes 1-3, there is an additional complication because of the partially formed resonance stabilization structure in the transition state. In some cases, the

pseudo double bond that is constrained in the allylic structure of the reactants might be released in the transition state, increasing the entropy. The higher pre-exponential factors for schemes 1 and 2 that are shown in [Figure 3a and 3b](#) are consistent with this.

For the cycloaddition reactions of alkenyl radicals, the following equation was shown to correlate the calculated pre-exponential factors with the number of frozen rotors (γ):

$$A(\text{s}^{-1}) = 2.36 \times 10^{13} \times e^{-2.11\gamma} \quad \text{eq (1)}$$

This relationship can be used to estimate the “effective” number of rotors loss ($\gamma_{\text{effective}}$) in the formation of the transition states for the reactions in schemes 1–3, where we simply substitute $\gamma_{\text{effective}}$ for γ in equation 1. The effective rotor loss can be determined from:

$$\gamma_{\text{effective}} = \gamma + \gamma_{\text{correction}} \quad \text{eq (2)}$$

Where, the corrected rotor loss ($\gamma_{\text{correction}}$) is determined by fitting the data to equation 1, the fit for the endo-cycloaddition alkenyl radical reactions. As mentioned above, for the exo-cycloaddition alkenyl radical reactions, $\gamma_{\text{correction}}$ is approximately -0.5 . For schemes 1-3, $\gamma_{\text{correction}}$ is determined to be approximately -0.5 for the endo-reactions and approximately -1.0 for the exo-pathways (which incorporates the factor of 0.5 for the C-C=C bending vibration). These results are summarized in [Table 7](#). For the endo-cycloaddition reactions of the alkenyl radicals, $\gamma_{\text{effective}}$ equals the number of frozen rotors (γ) in the transition state, which is straightforward to determine. To illustrate how this procedure works, let's consider the reaction of the C=CCC•C=C radical via scheme 1 (see reactions 1.1 and 1.5 in [Table 2](#)). If we count the rotation around the allylic bond, the reactant is considered to have three hindered rotors, and, regardless of the pathway, two of those rotors are lost in the formation transition state ring. Thus, for the endo pathway, $\gamma = 2$ and $\gamma_{\text{effective}} = 1.5$; for the exo-pathway, $\gamma = 2$ and $\gamma_{\text{effective}} = 1$. [Figure 3c and 3d](#) depicts the relationship between pre-exponential factors and $\gamma_{\text{effective}}$ for schemes 1-3. It shows that the pre-exponential factors group nicely with those for alkenyl radical reactions.

There have been several prior theoretical studies that have considered the endo- and exo-cycloaddition reactions of 1,5-hexadien-3-yl radical (C=CCC•C=C/C=CCC=CC•), particularly the reaction pathways that proceeds via scheme 3 (reactions 3.1 and 3.3 in [Table 4](#)). Cavallotti et al.³⁰, Sharma et al.⁴⁶, and Buras et al.⁴⁷ investigated the two cyclization pathways of the 1,5-hexadien-3-yl radical. Wu et al.¹⁹ studied the effects of substituents on the rate of intramolecular cyclization of the 1,5-hexadien-3-yl radical with DFT theory, using the UB3LYP functional. This reaction was also considered in our previous work³. The activation energies obtained in this study for these two pathways are consistent with those calculated by Sharma et al.⁴⁶ The rate constants calculated in this work are compared to those reported by Cavallotti et al.³⁰, Wu et al.¹⁹ and Buras et al.⁴⁷ in [Figure 4](#). Our rate constants and those of Buras et al.⁴⁷ are very similar for both the endo- and exo-reactions. The calculation by Wu et al.¹⁹ for the exo-pathway agrees fairly well with these two studies at lower temperatures. It's worth noting that these three studies

used very different theoretical methods. Cavallotti et al.³⁰ reported slightly higher rate constants, though they also showed that the exo-reaction has a higher rate constant than the endo-reaction.

Reactions of Non-resonant Linear Radicals

Tables 8-10 summarize the results for the alkyl-type dienyl radical reactions in schemes 4-6, respectively. For these reactions, the endo-pathway converts an alkenyl radical into a resonantly stabilized cyclic radical. Due to the gain of resonance-stabilization, this pathway is significantly exothermic. In contrast, the exo-pathway forms a non-stabilized cyclic carbonyl radical. The exo-reactions are endothermic for the 3- and 4-member rings, but become exothermic for the larger sized ring reactions. The investigated reactions in scheme 4 includes the 1,4 to 1,7 endo- and exo-reactions; for scheme 5 it includes the 1,5 to 1,7 reactions; and scheme 6 contains the 1,6 and 1,7 reactions. Again, the calculated rate constants are fit to modified Arrhenius form in 300-2500 K, and simple Arrhenius at 298 K and 500-1500 K. The modified fits are the preferred format when they are used for wide temperature ranges, since the pre-exponential factors show a substantial temperature dependence. The ring strain energies at 298 K are also provided; the energy barriers for the corresponding bimolecular reactions, which correspond to the addition of an alkyl radical to a diene, are provided in Table 11.

The activation energies for the reactions in schemes 4-6 are significantly lower than those for the corresponding reactions in schemes 1-3. However, the trends in the activation energies for all of the investigated reactions are similar. That is, for the endo-reactions in scheme 4 (Table 8), the activation energy decreases as the size of the ring formed in the transition state increases to a 6-membered ring. The activation energies for 1,6 reaction is just slightly less than the 1,7 reaction. For the exo-reactions, the activation energy for the 3-membered ring is less than that of the 4-membered ring reaction, but then the activation energies decrease as the ring size increases to the 6-membered ring. The activation energies for the endo- and exo- reactions of schemes 7 and 8 (Tables 9 and 10, respectively) are generally consistent with these observations.

The alkenyl cycloaddition reactions are again used as the reference reaction to analyze the influence of resonance stabilization on the activation energy. For the reactions in schemes 4-6 the bimolecular component of the barrier is ~5 kcal/mol lower in energy than that for the corresponding alkenyl reactions. The difference in the ring strain for the transition states in schemes 4-6 and those for the alkenyl radical reactions are shown in Figure 2. The ring strain energy for the endo-reactions of scheme 4 are lower than the alkenyl reactions, and the difference decreases as the transition state ring size increases. The strain energy for the endo-pathways of scheme 5 are smaller for the 5-member transition state ring and higher for the 6- and 7-member rings, than the corresponding alkenyl reactions. For scheme 6, the difference is smaller for the 6-membered ring reaction than it is for the 7-membered ring reaction. The ring strain for the exo-pathways of schemes 4-6 are all higher than the analogous alkenyl reactions. For the exo-pathways of scheme 4, the higher ring strain energies are primarily due to steric

effects that result from the presence of substituents on the reacting carbon atom in the double bond. For scheme 5, the partially-formed allylic structure distorts the bond angles and increase the strain energies; this impact is more significant for the smaller transition state ring size. For scheme 6, with the whole resonance structure inside the ring, the transition state structure it is further distorted, resulting in a higher strain energy. The optimized transition state structures for the reaction in schemes 4-6 are provided in [Figures S1 and S2](#) in the SI.

The pre-exponential factors for most of the reactions in schemes 4 and 5 are comparable to those for the analogous alkenyl reactions. For scheme 6, the pre-exponential factors are higher, due to a double bond that is contained within the transition state ring. The corrected number of rotors loss for the reactions in schemes 4-6 appears to be more complicated than those in schemes 1-3. These values are provided in [Table 7](#). Using these correction factors, the pre-exponential factors are plotted versus the effective rotor loss in [Figure 5](#), and the overall deviations among the various schemes is within a factor of 2 (as indicated by the blue dashed lines).

Reactions of Allyl Radical and Extended-Resonance Radicals

The reactions in [Table 12](#) represent three special cases (schemes 7-9). The reaction in scheme 7 is the cycloaddition reaction of allyl radical. The reactions in schemes 8 and 9 converts an extended resonantly stabilized linear radical to a regular resonantly stabilized cyclic radical for the endo-reaction and a non-resonant cyclic radical for the exo-reaction. These reactions resemble those in schemes 3 and 2, respectively. The reaction enthalpy changes are less exothermic than those in [Tables 2-4](#). The corresponding bimolecular reaction is that of stabilized radical addition to the conjugated diene forming a stabilized radical for the endo-reaction, and a non-stabilized radical for the exo-pathway; the calculated energy barriers are listed in [Table 11](#). For the formation of a given ring-size, the activation energies (as well as the ring strains) of these two type reactions are substantially higher than those for the reactions in schemes 1-3 and for the alkenyl radical reactions, for both the corresponding endo- and exo-pathways. The pre-exponential factors for these reactions are also higher than would be obtained using the usual correlations for schemes 3 and 2. These results suggest that the reactions involving extended resonance need to be treated individually.

Analysis of the C_6H_9 Potential Energy Surface

As shown above, the loss of the resonance stabilization in the reactant (e.g., schemes 1-3) means that the barriers for cyclization are significantly higher than those for the corresponding alkenyl radicals (cf. [Figure S1](#)). Despite this, however, these pathways still play an important role in the formation of molecular weight growth species. To illustrate this, in this section, we examine the addition reaction of vinyl plus 1,3-butadiene, which occurs on the C_6H_9 potential energy surface.

The relevant adduct on the C_6H_9 surface is the resonantly stabilized 1,5-hexadien-3-yl radical ($C=CCC=CC^*/C=CCC^*C=C$), which can react via schemes 1 and 3. The four competing pathways are shown in Figure 6. (The formation of the three membered ring via scheme 7 is not considered due to its high barrier.) The rate constant for exo-cycloaddition reaction by scheme 1 via a 3-membered ring transition state is higher than that for exo-cycloaddition by scheme 3 via a 4-membered ring transition state. Both of the exo-pathways are favored over the endo-reactions. Several prior studies have provided explanations as to why the exo-pathway is favored.^{12, 23, 25, 26} The activation energies for the 1,4 exo-reaction and 1,6 endo- and exo-reactions are comparable; the relative importance is determined by the pre-exponential factors. The 1,4 exo-pathway has the highest rate, followed by the 1,6 exo- and endo-reaction. The 1,4 endo-reaction has a much higher energy barrier than the other three pathways; it only become competitive at high temperatures (>1500 K).

Examination of the high-pressure rate constants shows that the exo-cycloaddition reaction of scheme 1 is favored over the other competing reactions. However, in order to understand the relative importance of these various pathways, one must consider other competing reaction channels from the adduct and the subsequent reactions from the cyclized isomers. A simplified version of the C_6H_9 potential energy surface³ is shown in Figure 7. Some of the pathways on this surface have been reported by Buras et al.⁴⁷ (at the CCSD(T)-F12a/cc-pVTZ-F12 level of theory). Cyclization of 1,5-hexadien-3-yl (1) by the endo-pathways lead to (6) and (3) via schemes 1 and 3, respectively. The exo-pathways leads to (7) and (4), respectively. Species (7) can ring-open to form the branched adduct (8), which can cyclize to form (9). These types of isomerization pathways have previously been discussed.⁴⁸ The 1,5-hexadien-3-yl (1) can also undergo an intramolecular H-atom shift reaction to form the 1,3-hexadien-5-yl (2), which can cyclize via the endo- and exo-reactions of scheme 3 to form (5) and (10), respectively.

Analysis of the C_6H_9 surface shows that: *a*) The barriers for all of the cycloaddition reactions, and for the H-atom shift reactions, are generally lower in energy than barriers for the corresponding competing β -scission of the adducts (e.g., (1) to (VII) and (VIII), (2) to (VII), and (3) to (III) and (IV)), although the pre-exponential factors are notably lower. *b*) As shown above, the exo-cycloaddition of (1) to (7) has the lowest barrier. However, the cyclic isomer (7) is more likely to ring open (either back to (1) or to (8)) than it is to directly β -scission to (XIII). *c*) The scheme 1 cycloaddition reactions of (1) to (3) and (4) have comparable energy barriers. The subsequent reactions from (3) to (III) and (IV) correspond to the lowest energy exit channels, followed by the reaction of (4) to (5) then to (I). *d*) If the surface is entered from the addition of vinyl to 1,3-butadiene (VIII), then the adduct (1) is chemically activated and it has sufficient energy to directly react to form the stable unsaturated 5- and 6-membered ring species.

The chemically-activated pressure dependent rate constants for the reaction of vinyl plus 1,3-butadiene to form adduct (1) at 1 atm are shown by the solid lines in Figure 8. Note that the figure is divided into two plots for readability; on the left hand side are the rate constants to form

the collisionally-stabilized intermediate radicals and on the right-hand side are the rate constants to form bimolecular products. The rate constants forming the products, including cyclohexadiene isomers + H (III) and (IV), and cyclopentadiene + CH₃ (I), are significant, especially at ~1000K. Thus, even though the formation of the partial resonance structure in the transition state, increases the activation energy (compared to the alkenyl radical cycloadditions), the energy of the entrance channels is sufficiently high that the cycloaddition reactions and the subsequent β -scission reactions are accessible, effectively “locking in” the molecular weight growth products.

Our earlier study³ presented an approximate method for the analysis of complex pressure-dependent reaction systems involving alkyl radical H-atom shift and alkenyl radical cycloaddition reactions. This study as well as a previous one²⁷ investigated the impact of resonance stabilization on these two type isomerization reactions for radicals with unsaturated bond(s). Together they allow us now to extend the approximate method to more complicated reaction systems. This method has been applied to the C₆H₉ potential energy surface in [Figure 7](#). The estimated energies are compared to the CBS-QB3 results in [Table S4](#) in the SI. The activation energy for the H-atom shift reactions (i.e., species (1) to (2) and (4) to (5)) are estimated from the sum of energy barrier of the analogous H-abstraction reaction and ring strain.^{23, 27} Similarly, the activation energy for the cycloaddition reactions (i.e., species (1) to (4) and (3), (2) to (5), and (8) to (9)) are estimated from the sum of analogous addition reactions and ring strain, which have been discussed above as well as in our prior study.^{3, 23} The barriers of the addition reactions for the entrance and exit channels are estimated from similar reactions in the literature.^{41, 49-51} In each case, the rate parameters for the reverse reactions were obtained from the estimated rate parameters for the forward reaction and the group additivity based equilibrium constant. Comparison of the estimated and calculated results reveals that, in most cases, the estimated enthalpies using group additivity methods^{36, 37} for the stable species are lower than the calculated values. The enthalpies for the transition states are also lower, meaning that estimated and calculated barriers are quite similar. For three species (6, 9, and X) the estimated enthalpies are ~5-10 kcal/mol lower than the corresponding calculated values. However, there is only one transition state (10-X) where the difference in barriers is greater than ~3 kcal/mol. [Figure 8](#) shows the apparent rate constants at 1 atm based on the estimated values (dashed lines) as well as these obtained from CBS-QB3 calculations (solid lines) for reaction of vinyl plus 1,3-butadiene (VIII) via the chemically activated 1,5-hexadien-3-yl radical (1). Overall, the results derived from the approximate surface are reasonably consistent with the more rigorous treatment.

Summary

The influence of the resonance structure on the kinetics of endo- and exo-cycloaddition reactions was examined using electronic structure calculations at the CBS-QB3 level of theory. The results are discussed in the context of a Benson-type model to examine the impact on both the activation energies (including ring strain) and pre-exponential factors. Two sets of reactions

were investigated. In the first set, a resonant linear dienyl radical is converted into a non-resonant cyclic radical. In the second set, a non-allylic linear dienyl radical is converted to either an allylic cyclic radical or a cyclic carbinyl radical. In each case, three different reaction schemes are examined based on the location of the resonance structure in the cyclic transition state. The results are compared to previously reported rate parameters for the cycloaddition reactions of alkenyl radicals. For the endo-pathways, the activation energies for the first and second sets reactions are higher and lower, respectively, than those for the corresponding alkenyl radical reactions. For the exo-pathways, the activation energies for both sets reactions are higher than the alkenyl reactions. These differences are primarily due to the bimolecular component of the activation energy in the Benson-type model, which in turn is governed by the different reaction enthalpies. However, in some cases, the presence of the partially-formed resonance structure in transition state significantly increases the transition state ring strain energy. The pre-exponential factors are also impacted by the formation of allylic transition state structures. Comparison of the investigated schemes to those of analogous alkenyl reactions indicate the partially-formed transition state resonant structures have a profound impact on the overall reaction rates. Thus, it is important to be able to account for the impact of the full and/or partial resonance in rate estimation methods. To facilitate this, we have provided correction factors (in the form of ring strains and corrected rotors) that can be used to generate rate estimation rules. The improved understanding of the impact of resonance stabilization on unimolecular isomerization reactions is used to generate estimates of the rate constants for the reactions that occur on the C_6H_9 potential energy surface. Such an extension is important for the development of kinetic mechanisms, especially in the context of molecular weight growth during the pyrolysis and oxidation of olefins and alkanes. The analysis of the addition reaction of vinyl to 1,3-cyclopentadiene on the C_6H_9 surface reveals that the cycloaddition channels are an energetically favorable route to the formation of molecular weight growth species.

Acknowledgements

The authors wish to thank Dr. Hans-Heinrich Carstensen at Ghent University for assistance with the rate constant calculations. This work was supported by the Petroleum Institute and the National Advanced Biofuels Consortium.

Supporting information

Comparison of activation energies at 298K for H-atom shift reactions in schemes 1-6 for different transition state ring sizes to those of analogous alkyl radical reactions (Figure S1). Transition state structures for the various cycloaddition reactions in schemes 1-6 and alkenyl radicals for the endo- and exo-pathways (Figure S2 and S3, respectively). Additional calculated reactions for schemes 1-3 (Tables S1-S3, respectively). The estimated and calculated energies for species and transition state in the C_6H_9 potential energy surface (Table S4). This information is available free of charge via the internet at....

References

- 1 K. L. Randolph, A. M. Dean, *Phys. Chem. Chem. Phys.*, 2007, **9**, 4245–4258.
- 2 C. Xu, A. S. Al-Shoaibi, C. G. Wang, H.-H. Carstensen and A. M. Dean, *J. Phys. Chem. A*, 2011, **115**, 10470–10477.
- 3 K. Wang, S. M. Villano and A. M. Dean, *Phys. Chem. Chem. Phys.*, 2015, **15**, 6255–6273.
- 4 K. D. King, *Inter. J. Chem. Kinetics*, 1978, **10**, 117–123.
- 5 D. K. Lewis, M. Sarr, M. Keil, *J. Phys. Chem.*, 1974, **78**, 436–439.
- 6 D. K. Lewis, J. Bergmann, R. Manjoney, R. Paddock and B. L. Kaira, *J. Phys. Chem.*, 1984, **88**, 4112–4116.
- 7 R. G. Butler and I. Glassman, *Proc. Combust. Inst.*, 2009, **32**, 395–402.
- 8 D. H. Kim, J. A. Mulholland, D. Wang and A. Violi, *J. Phys. Chem. A*, 2010, **114**, 12411–12416.
- 9 C. Cavallotti, D. Polino, A. Frassoldati and E. Ranzi, *J. Phys. Chem. A*, 2012, **116**, 3313–3324.
- 10 M. R. Djokic, K. M. Van Geem, C. Cavallotti, A. Frassoldati, E. Ranzi and G. B. Marin, *Combust. Flame*, 2014, **161**, 2739–2751.
- 11 D. Wang, A. Violi, D. H. Kim and J. A. Mullholland, *J. Phys. Chem. A*, 2006, **110**, 4719–4725.
- 12 J. E. Baldwin, *J. Chem. Soc., Chem. Commun.*, 1976, 734–736.
- 13 C. Chatgililoglu, K. U. Ingold and J. C. Scaiano, *J. Am. Chem. Soc.*, 1981, **103**, 7739–7742.
- 14 S. M. Handford-Styring and R. W. Walker, *J. Chem. Soc. Faraday Trans.*, 1995, **91**, 1431–1438.
- 15 P. A. Arnold and B. K. Carpenter, *Chem. Phys. Lett.*, 2000, **328**, 90–96.
- 16 A. L. Cooksy, H. F. King, W. H. Richardson, *J. Org. Chem.*, 2003, **68**, 9441–9452.
- 17 D. M. Matheu, W. H. Green and J. M. Grenda, *Int. J. Chem. Kinet.*, 2003, **35**, 95–119.
- 18 W. Tsang, *J. Phys. Chem. A*, 2006, **110**, 8501–8509.
- 19 C.-W. Wu, H.-L. Chen, and J.-J. Ho, *J. Mol. Struct.: Theochem.*, 2007, **815**, 11–20.
- 20 B. Sirjean, P. A. Glaude, M. F. Ruiz-Lopèz and R. Fournet, *J. Phys. Chem. A*, 2008, **112**, 11598–11610.
- 21 I. A. Awan, D. R. Jr. Burgess, J. A. Manion, *J. Phys. Chem. A*, 2012, **116**, 2895–2910.
- 22 H. T. Bian, Z. H. Wang, F. Zhang, Z. D. Wang and J. P. Zhu, *Inter. J. Chem. Kinetics*, 2015, **47**, 685–694.
- 23 K. Wang, S. M. Villano and A. M. Dean, *J. Phys. Chem. A*, 2015, **119**, 7205–7221.
- 24 S. W. Benson, *Thermochemical Kinetics*, 2nd ed.; Wiley: New York, 1976.
- 25 A. L. J. Beckwith, *Tetrahedron*, 1981, **31**, 3073–3100.
- 26 A. L. J. Beckwith and C. H. Schiesser, *Tetrahedron Lett.* 1985, **26**, 373–376.
- 27 K. Wang, S. M. Villano and A. M. Dean, *ChemPhysChem*, 2015, **16**, 2635–2645.

-
- 28 M. Saeys, M. F. Reyniers, G. B. Marin, V. Van Speybroeck and M. Waroquier, *J. Phys. Chem. A*, 2003, **107**, 9147–9159.
- 29 M. Saeys, M. F. Reyniers, G. B. Marin, V. Van Speybroeck and M. Waroquier, *AIChE J.*, 2004, **50**, 426–444.
- 30 C. Cavallotti, S. Fascella, R. Rota and S. Carra, *Combust. Sci. Technol.*, 2004, **176**, 705–720.
- 31 M. J. Frisch, G. W. Trucks, H. B. Schlegel, G. E. Scuseria, M. A. Robb, J. R. Cheeseman, J. A., Jr. Montgomery, T. Vreven, K. N. Kudin and J. C. Burant, et al., Gaussian 03, Revision A. 1, Gaussian, Inc: Pittsburgh, PA, 2003.
- 32 M. J. Frisch, G. W. Trucks, H. B. Schlegel, G. E. Scuseria, M. A. Robb, J. R. Cheeseman, G. Scalmani, V. Barone, B. Mennucci and G. A. Petersson, et al., Gaussian 09, Revision A. 1, Gaussian, Inc: Wallingford, CT, 2009.
- 33 J. J. A. Montgomery, M. J. Frisch, J. W. Ochterski and G. A. Petersson, *J. Chem. Phys.*, 2000, **112**, 6532–6542.
- 34 A. L. L. East and L. Radom, *J. Chem. Phys.* 1997, **106**, 6655–6674.
- 35 C. Eckart, *Phys. Rev.*, 1930, **35**, 1303–1309.
- 36 E. R. Ritter and J. W. Bozzelli, *Int. J. Chem. Kinetics*, 1991, **23**, 767–778.
- 37 http://rmg.mit.edu/molecule_search
- 38 J. Troe, *Ber. Bunsen-Ges. Phys. Chem.*, 1983, **87**, 161–169.
- 39 A. Y. Chang, J. W. Bozzelli and A. M. Dean, *Z. Phys. Chem.*, 2000, **214**, 1533–1568.
- 40 H. Richter and J. B. Howard, *Phys. Chem. Chem. Phys.*, 2002, **4**, 2038–2055
- 41 H.-H. Carstensen and A. M. Dean, In *Comprehensive Chemical Kinetics*; ed. R. Carr, Elsevier: New York, 2007, **42**, 105–187.
- 42 S. M. Villano, H.-H. Carstensen and A. M. Dean, *J. Phys. Chem. A*, 2013, **117**, 6458–6473.
- 43 C. Sheng, Ph. D. Dissertation, New Jersey Institute of Technology, 2002.
- 44 K. P. Somers, Ph. D. Dissertation, National University of Ireland, Galway, 2014
- 45 H.-H. Carstensen and A. M. Dean, *Int. J. Chem. Kinet.*, 2011, **44**, 75–89.
- 46 S. Sharma, M. R. Harper and W. H. Green, *Combust. Flame*, 2010, **157**, 1331–1345.
- 47 Z. J. Buras, E. E. Dames, S. S. Merchant, G. Z. Liu, R. M. I. Elsamra, and W. H. Green, *J. Phys. Chem. A*, **2015**, 119, 7325–7338.
- 48 Z. H. Wang, L. D. Zhang, F. Zhang, *J. Phys. Chem. A* 2014, **118**, 6741–6748.
- 49 W. Tsang, *J. Phys. Chem. Ref. Data*, 1991, **20**, 221–273.
- 50 M. K. Sabbe, A. G. Vandeputte, M. F. Reyniers, V. V. Speybroeck, M. Waroquier and G. B. Marin, *J. Phys. Chem. A*, 2007, **111**, 8416–8428.
- 51 M. K. Sabbe, M. F. Reyniers, V. V. Speybroeck, M. Waroquier and G. B. Marin, *ChemPhysChem*, 2008, **9**, 124–140.

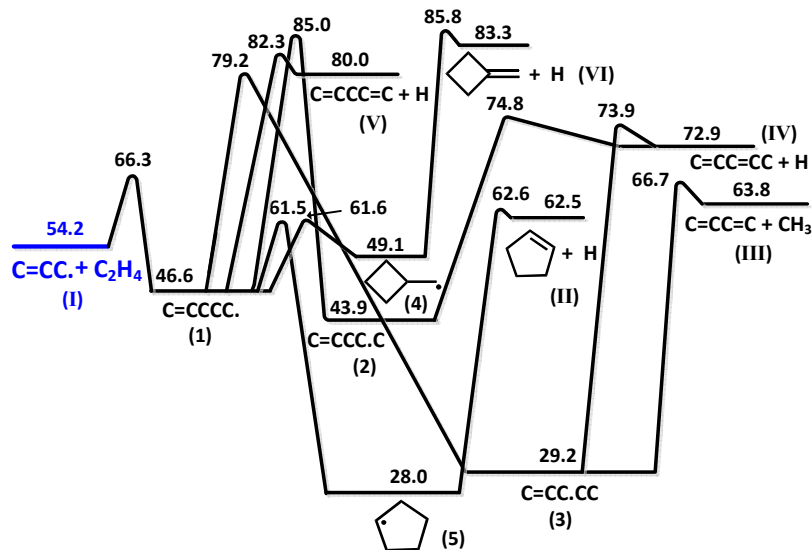


Figure 1: Simplified C_5H_9 potential energy surface at the CBS-QB3 level of theory, showing the enthalpies in kcal/mol at 298K³. (Reprint with permission from PCCP)

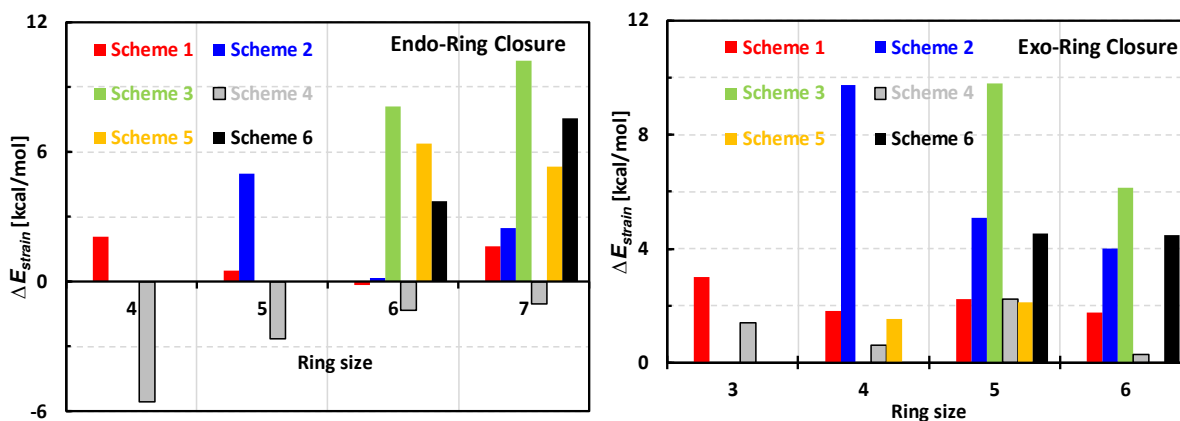


Figure 2: Comparison of the differences in ring strain energies of endo- (left) and exo- (right) cycloaddition reactions in schemes 1-6 for different transition state ring sizes to those of analogous alkenyl radical reactions²³ at 298K.

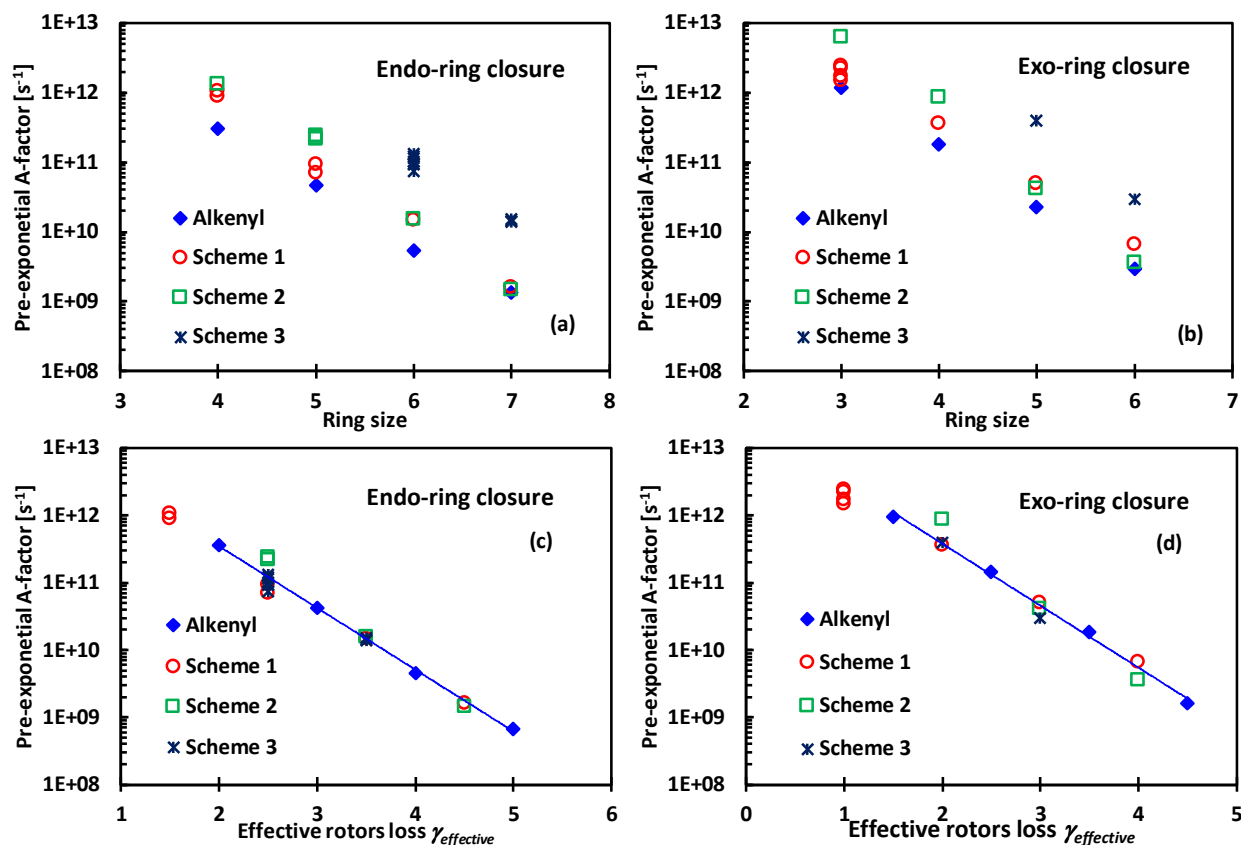


Figure 3: The pre-exponential factors versus the ring size of transition states (a and b) and effective rotor loss (c and d) in temperature range of 500-1500 K. (Open and crossed symbols: Schemes 1-3 in this study; filled blue symbols and blue line: ring closure reactions of alkenyl radicals from the previous work²³).

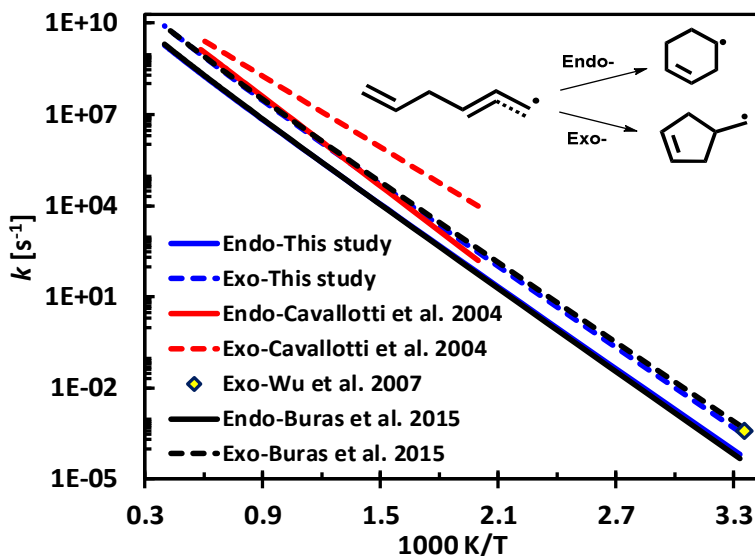


Figure 4: Comparison of the reported rate constants for endo- and exo-ring closure reactions of the 1,5-hexadien-3-yl radical (C=CCC=CC•/C=CCC•C=C) and this study.

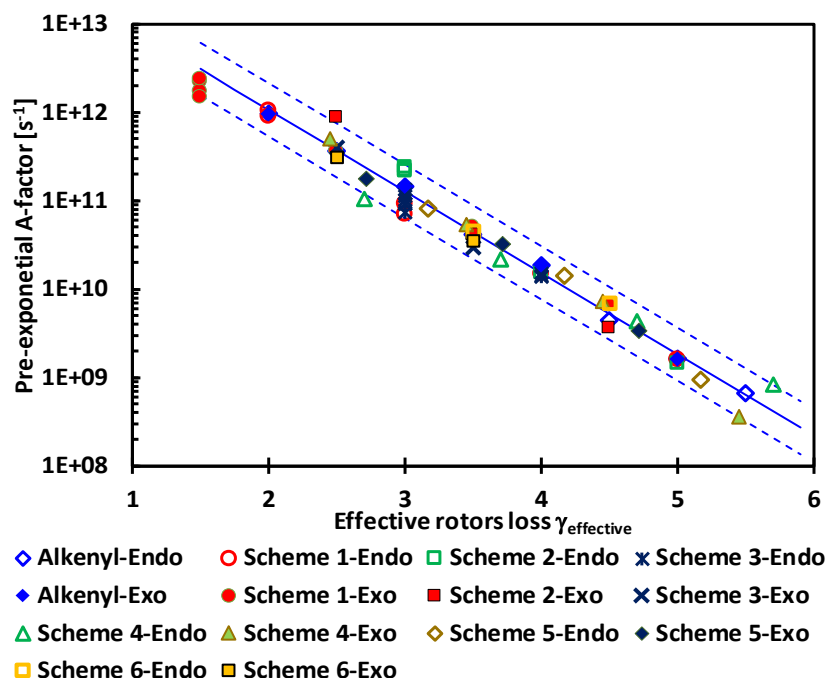


Figure 5: Correlation between the pre-exponential factors and effective loss of hindered rotors ($\gamma_{\text{effective}}$) in temperature range of 500-1500 K. (Blue symbols and blue solid line—Ring closure of alkenyl radicals from the previous work²³, Upper and lower dashed lines— The pre-exponential factors calculated by the correlation multiply and divided by a factor of 2; Symbols in other colors—Schemes 1-6 in this study).

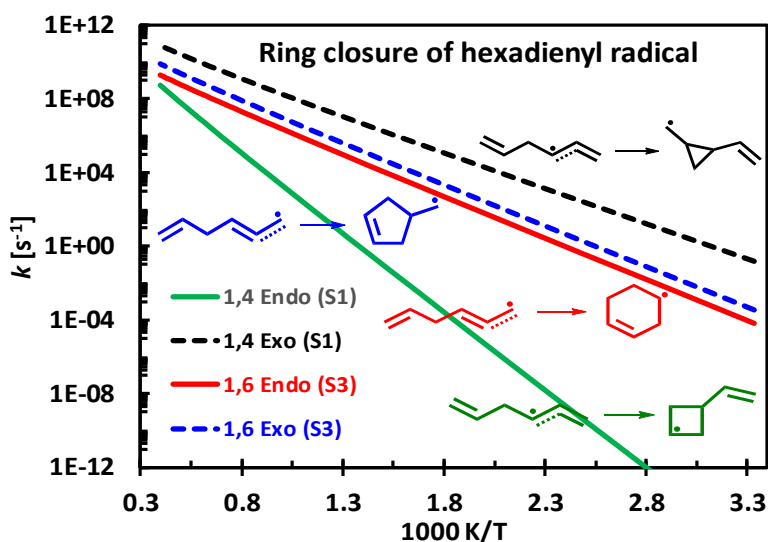


Figure 6: Comparison of the rate constants for the various cycloaddition pathways for the 1,5-hexadien-3-yl radical ($\text{C}=\text{CCC}=\text{CC}^{\bullet}/\text{C}=\text{CCC}^{\bullet}\text{C}=\text{C}$). Note that S1 and S3 mean schemes 1 and 3, respectively.



Figure 7: Simplified C_6H_9 potential energy surface calculated at the CBS-QB3 level of theory, showing the enthalpies in kcal/mol at 298K. The cycloaddition reactions are shown by the blue lines (scheme 3), red lines (scheme 1), and the purple lines. For these reactions the dashed lines correspond to the exo-pathway and the solid lines to the endo-pathway. The blue lines correspond to H-atom shift reactions and the black lines to β -scission reactions.

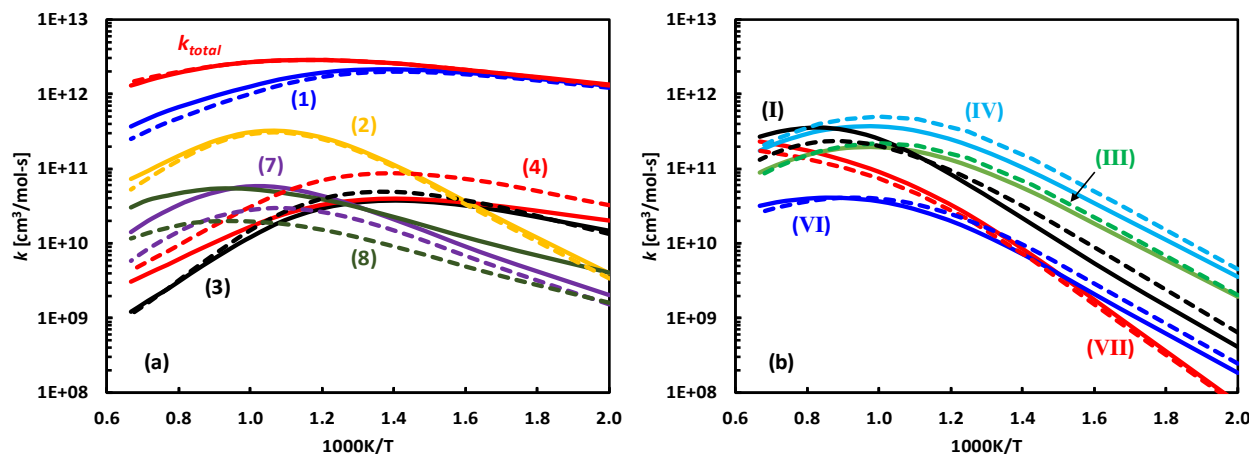


Figure 8: Comparison of the predicted chemically activated rate constants based on CBS-QB3 calculations (solid lines with symbols) to those estimated using rate rules (dashed lines) for the product channels resulting from the addition reaction of vinyl to 1,3-butadiene (VIII in Figure 7) at 1 atm in N_2 . The left-hand side plot shows the rate constants to form the adducts and the right-hand side shows the rate constants to form bimolecular products. The product structures are provided in Figure 7: (1) $\text{C}=\text{CCC}=\text{CC}\cdot$, (2) $\text{C}=\text{CC}=\text{CC}\cdot\text{C}$, (3) cyclohexene-4-yl, (4) cyclopentene-4-carbinyl, (7) 1-vinyl-cyclopentane-2-carbinyl, (8) 2-vinyl-1-butenyl, (I) 1,3-cyclopentadiene + CH_3 , (III) 1,3-cyclohexadiene + H, (IV) 1,4-cyclohexadiene + H, (VI) methylene-cyclopentene + H, and (VII) $\text{H} + \text{C}=\text{CC}=\text{CC}=\text{C}$.)

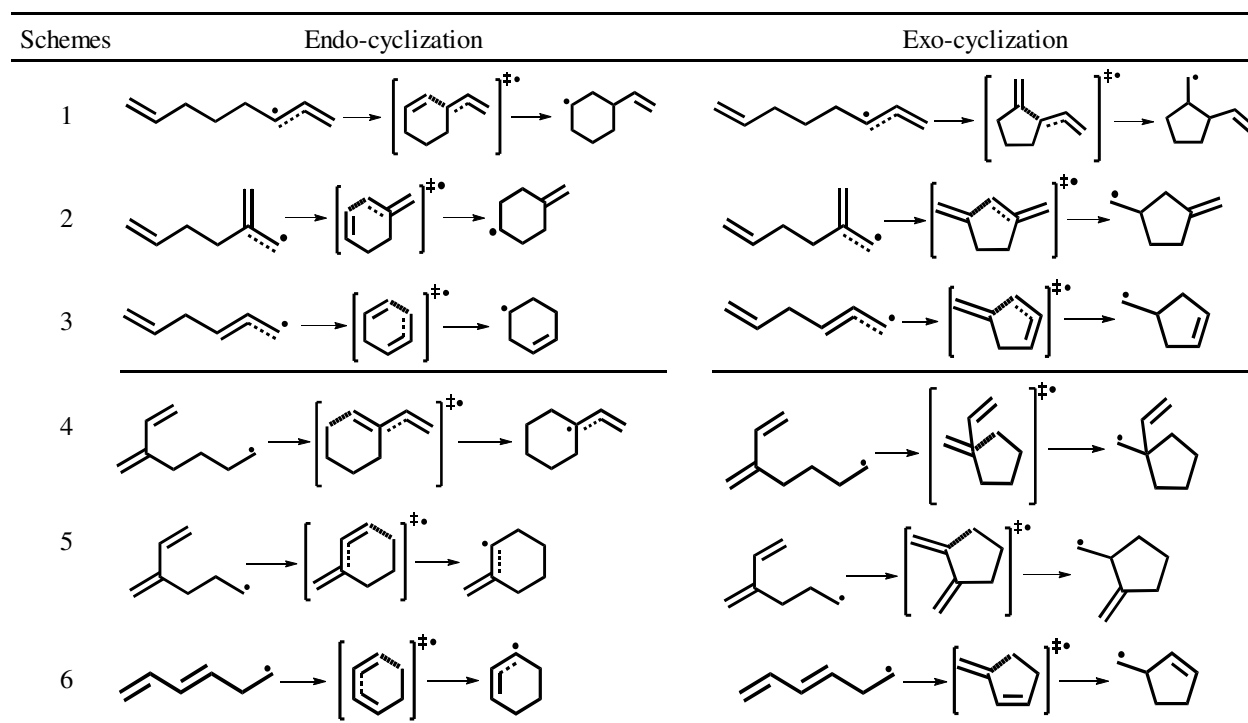
Table 1: Representative reactions for schemes 1-6.

Table 2: Rate Constants and Reaction Enthalpies Calculated at CBS-QB3 Level of Theory for the Endo- and Exo-ring Closure Reactions of Scheme 1.

#	Reactants	300-2500 K			500-1500 K		298 K		E_{strain}	$\Delta_R H^{298}$
		Modified Arrhenius Parameters			Arrhenius Parameters		Arrhenius Parameters			
		A	n	E	A''	E_a'	A'	E_a		
1.1	1,4 Endo C=CCC•C=C									
		6.03E+07	1.25	37.6	1.05E+12	39.7	2.66E+11	38.3	26.6	19.2
1.2	1,5 Endo C=CCCC•C=C									
		1.70E+07	1.10	19.8	9.24E+10	21.7	2.76E+10	20.5	8.8	-3.8
1.3	1,6 Endo C=CCCCC•C=C									
		4.14E+05	1.34	11.7	1.46E+10	13.9	3.30E+09	12.5	0.8	-6.4
1.4	1,7 Endo C=CCCCCC•C=C									
		9.25E+04	1.25	13.3	1.60E+09	15.4	4.06E+08	14.0	2.3	-3.4
1.5	1,4 Exo C=CCC•C=C									
		3.28E+08	1.13	16.6	2.23E+12	18.5	6.33E+11	17.3	4.7	16.5
1.6	1,5 Exo C=CCCC•C=C									
		4.97E+06	1.44	20.7	3.61E+11	23.1	7.47E+10	21.6	9.0	17.2
1.7	1,6 Exo C=CCCCC•C=C									
		7.66E+05	1.42	11.7	5.02E+10	14.1	1.05E+10	12.5	-0.1	-0.5
1.8	1,7 Exo C=CCCCCC•C=C									
		9.55E+04	1.34	11.6	3.33E+09	13.8	7.64E+08	12.4	-0.2	-5.2

Note: ^a The units for A, A', and A'' are s⁻¹, and are kcal/mol for $\Delta_R H^{298}$, E, E_a , E_a' , and E_{strain} . ^b Molecule structures are presented in abbreviated form (H atoms missing, radical site marked with “•”) to improve readability.

Table 3: Rate Constants and Reaction Enthalpies Calculated at CBS-QB3 Level of Theory for the Endo- and Exo-ring Closure Reactions of Scheme 2.

#	Reactants	300-2500 K			500-1500 K		298 K		E_{strain}	$\Delta_R H^{298}$	
		Modified Arrhenius Parameters			Arrhenius Parameters		Arrhenius Parameters				
		A	n	E	A''	E_a'	A'	E_a			
2.1	1,5 Endo $C=C(C\bullet)CC=C$		4.35E+08	0.80	24.2	2.20E+11	25.6	9.17E+10	24.7	13.3	-4.3
2.2	1,6 Endo $C=C(C\bullet)CCC=C$		1.96E+07	0.86	11.8	1.54E+10	13.2	6.01E+09	12.3	0.9	-8.7
2.3	1,7 Endo $C=C(C\bullet)CCCC=C$		8.02E+05	0.98	13.9	1.46E+09	15.3	5.64E+08	14.5	3.1	-5.4
2.4	1,5 Exo $C=C(C\bullet)CC=C$		8.33E+08	0.89	29.0	8.64E+11	30.5	3.25E+11	29.5	16.9	17.3
2.5	1,6 Exo $C=C(C\bullet)CCC=C$		2.75E+07	0.94	14.8	4.11E+10	16.4	1.47E+10	15.3	2.7	-3.2
2.6	1,7 Exo $C=C(C\bullet)CCCC=C$		1.11E+06	1.05	14.0	3.60E+09	15.6	1.27E+09	14.6	2.0	-3.2

Note: ^a The units for A, A', and A'' are s^{-1} , and are kcal/mol for $\Delta_R H^{298}$, E, E_a , E_a' , and E_{strain} . ^b Molecule structures are presented in abbreviated form (H atoms missing, radical site marked with “•”) to improve readability.

Table 4: Rate Constants and Reaction Enthalpies Calculated at CBS-QB3 Level of Theory for the Endo- and Exo-ring Closure Reactions of Scheme 3.

#	Reactants	300-2500 K			500-1500 K		298 K		E_{strain}	$\Delta_R H^{298}$	
		Modified Arrhenius Parameters			Arrhenius Parameters		Arrhenius Parameters				
		A	n	E	A''	E_a'	A'	E_a			
3.1	1,6 Endo $C=CCC=CC\bullet$		2.31E+08	0.78	19.9	1.02E+11	21.2	4.32E+10	20.3	8.9	-7.2
3.2	1,7 Endo $C=CCCC=CC\bullet$		7.89E+06	0.87	21.8	7.11E+09	23.3	2.73E+09	22.3	10.9	-3.4
3.3	1,6 Exo $C=CCC=CC\bullet$		4.71E+08	0.86	19.6	3.93E+11	21.0	1.52E+11	20.1	7.5	-2.0
3.4	1,7 Exo $C=CCCC=CC\bullet$		7.14E+06	0.93	16.2	9.88E+09	17.8	3.57E+09	16.7	4.1	-6.6

Note: ^a The units for A, A', and A'' are s^{-1} , and are kcal/mol for $\Delta_R H^{298}$, E, E_a , E_a' , and E_{strain} . ^b Molecule structures are presented in abbreviated form (H atoms missing, radical site marked with “•”) to improve readability.

Table 5: The Reference Bimolecular Addition Reactions of Allylic Radicals to Olefins for Schemes 1-3.

Reactions	A [cm ³ /mol-s]	n	E [kcal/mol]	E _a (298 K) [kcal/mol]	Δ _R H ²⁹⁸ [kcal/mol]
Terminal addition					
C=CC• + C ₂ H ₄ ↔ C=CCCC•	2.70E+03	2.7	11.3	12.1	-7.5
CC=CC• + C ₂ H ₄ ↔ trans-CC=CCCC•	5.04E+02	2.7	11.6	12.3	-7.2
C=C(C)C• + C ₂ H ₄ ↔ C=C(C)CCC•	2.16E+03	2.7	10.3	11.0	-8.3
C=CC• + C=CC ↔ C=CCCC•C	1.56E+03	2.5	11.0	11.7	-7.9
C=CC• + C=CCC ↔ C=CCCC•CC	1.31E+03	2.6	10.9	11.6	-7.5
C=C(C)C• + C=C(C)C ↔ C=C(C)CCC(C)•C	5.20E+03	2.5	9.3	10.0	-8.1
			Average	11.4	
			STDEV	0.9	
C=CC•C + C ₂ H ₄ ↔ C=CC(C)CC•	1.01E+02	3.0	11.3	12.0	-6.5
C=CC•C + C=CC ↔ C=CC(C)CC•C	5.42E+01	2.9	10.6	11.3	-6.7
			Average	11.7	
			STDEV	0.5	
Non-terminal addition					
C=CC• + C=CC ↔ C=CCCC ₂ •	1.37E+02	2.8	12.2	12.9	-5.7
C=CC• + C=CCC ↔ C=CCC(C•)CC	1.22E+01	3.1	11.7	12.5	-6.7
C=CC• + trans-CC=CC ↔ C=CCC ₂ C•C	9.53E+02	2.7	11.2	12.0	-6.4
C=C(C)C• + C=C(C)C ↔ C=C(C)CCC ₃ •	2.75E+00	3.2	12.3	13.1	-4.2
			Average	12.6	
			STDEV	0.5	
C=CC•C + C=CC ↔ C=CC(C)CC(C)•	1.71E+00	3.2	11.7	12.6	-3.9

Note: The Arrhenius parameters are obtained in T=300-2500 K.

Table 6: Rate Constants and Reaction Enthalpies Calculated at CBS-QB3 Level of Theory for the Endo- and Exo-ring Closure Reactions of the Alkenyl Radicals.

#	Reactants	300 - 2500 K			500 - 1500 K		298 K		E_{strain}	$\Delta_R H^{298}$
		Modified Arrhenius Parameters			Arrhenius Parameters		Arrhenius Parameters			
		A	n	E	A''	E_a'	A'	E_a		
	1,4 Endo									
1	C=CCC•	6.60E+07	1.08	30.4	3.08E+11	32.2	9.38E+10	31.0	24.5	4.6
	1,5 Endo									
2	C=CCCC•	1.65E+07	1.02	14.2	4.68E+10	15.9	1.53E+10	14.8	8.3	-18.5
	1,6 Endo									
3	C=CCCCC•	1.25E+06	1.08	6.7	5.44E+09	8.5	1.67E+09	7.3	0.8	-22.1
	1,7 Endo									
4	C=CCCCC•	1.14E+05	1.20	6.5	1.36E+09	8.5	3.62E+08	7.2	0.7	-19.6
	1,4 Exo									
5	C=CCC•	6.32E+08	0.97	8.9	1.19E+12	10.5	4.13E+11	9.5	1.7	2.5
	1,5 Exo									
6	C=CCCC•	2.07E+06	1.46	14.1	1.81E+11	16.6	3.65E+10	15.0	7.2	2.5
	1,6 Exo									
7	C=CCCCC•	6.98E+05	1.33	4.7	2.26E+10	6.9	5.24E+09	5.5	-2.3	-15.7
	1,7 Exo									
8	C=CCCCC•	1.53E+05	1.26	5.1	2.91E+09	7.2	7.28E+08	5.8	-2.0	-22.6

Note: ^a The units for A, A', and A'' are s⁻¹, and are kcal/mol for $\Delta_R H^{298}$, E, E_a , E_a' , and E_{strain} . ^b Molecule structures are presented in abbreviated form (H atoms missing, radical site marked with “•”) to improve readability.

Table 7: Summary of Corrected Rotors Loss ($\gamma_{correction}$) for Different Reaction Schemes.

Reaction types	Corrected rotors loss ($\gamma_{correction}$)		Note
	Endo-cycloaddition	Exo-cycloaddition	
Alkenyl radicals	0	-0.5	By definition (endo-reaction)
Schemes 1-3	-0.5	-1.0	Resonantly-stabilized linear radical to non-resonant cyclic radicals
Scheme 4	0.2	0.5	Non-resonantly-stabilized linear radical to resonant (endo-reaction) or non-resonant carbonyl cyclic (exo-reaction) radicals
Scheme 5	-0.3	-0.3	
Scheme 6	0	0	

Table 8: Rate Constants and Reaction Enthalpies Calculated at CBS-QB3 Level of Theory for the Endo- and Exo-ring Closure Reactions of Scheme 4.

#	Reactants	300-2500 K			500-1500 K		298 K		E_{strain}	$\Delta_R H^{298}$	
		Modified Arrhenius Parameters			Arrhenius Parameters		Arrhenius Parameters				
		A	n	E	A''	E_a'	A'	E_a			
4.1	1,4 Endo C=C(C=C)CC•		3.64E+08	0.73	22.5	1.04E+11	23.7	4.71E+10	22.9	19.0	-8.5
4.2	1,5 Endo C=C(C=C)CC•		9.29E+06	0.99	9.0	2.13E+10	10.7	7.18E+09	9.6	5.7	-30.9
4.3	1,6 Endo C=C(C=C)CCC•		8.82E+05	1.09	2.7	4.31E+09	4.5	1.31E+09	3.4	-0.5	-34.6
4.4	1,7 Endo C=C(C=C)CCCC•		8.92E+04	1.17	2.9	8.33E+08	4.8	2.30E+08	3.6	-0.3	-31.5
4.5	1,4 Exo C=C(C=C)CC•		5.92E+09	0.57	10.9	5.03E+11	11.8	2.77E+11	11.3	3.1	5.9
4.6	1,5 Exo C=C(C=C)CC•		5.37E+07	0.89	15.5	5.39E+10	16.9	2.11E+10	16.0	7.8	6.2
4.7	1,6 Exo C=C(C=C)CCC•		9.27E+06	0.87	7.6	7.17E+09	8.8	3.12E+09	8.1	-0.1	-12.0
4.8	1,7 Exo C=C(C=C)CCCC•		1.64E+05	1.01	5.9	3.60E+08	7.3	1.40E+08	6.5	-1.7	-17.4

Note: ^a The units for A, A', and A'' are s⁻¹, and are kcal/mol for $\Delta_R H^{298}$, E, E_a , E_a' , and E_{strain} . ^b Molecule structures are presented in abbreviated form (H atoms missing, radical site marked with “•”) to improve readability.

Table 9: Rate Constants and Reaction Enthalpies Calculated at CBS-QB3 Level of Theory for the Endo- and Exo-ring Closure Reactions of Scheme 5.

#	Reactants	300-2500 K			500-1500 K		298 K		E_{strain}	$\Delta_R H^{298}$	
		Modified Arrhenius Parameters			Arrhenius Parameters		Arrhenius Parameters				
		A	n	E	A''	E_a'	A'	E_a			
5.1	1,5 Endo C=C(C=C)CC•		7.48E+08	0.61	11.9	8.02E+10	12.7	4.48E+10	12.2	8.3	-30.0
5.2	1,6 Endo C=C(C=C)CC•		9.77E+07	0.65	10.7	1.39E+10	11.5	7.80E+09	11.1	7.2	-33.2
5.3	1,7 Endo C=C(C=C)CCC•		3.34E+06	0.75	9.5	9.55E+08	10.4	5.04E+08	9.9	6.0	-31.0
5.4	1,5 Exo C=C(C=C)CC•		1.24E+09	0.65	16.5	1.78E+11	17.5	9.49E+10	16.9	8.7	6.1
5.5	1,6 Exo C=C(C=C)CC•		2.72E+07	0.92	7.4	3.19E+10	8.8	1.29E+10	8.0	-0.2	-13.5
5.6	1,7 Exo C=C(C=C)CCC•		4.00E+06	0.88	5.6	3.38E+09	6.8	1.50E+09	6.2	-2.0	-18.6

Note: ^a The units for A, A', and A'' are s⁻¹, and are kcal/mol for $\Delta_R H^{298}$, E, E_a , E_a' , and E_{strain} . ^b Molecule structures are presented in abbreviated form (H atoms missing, radical site marked with “•”) to improve readability.

Table 10: Rate Constants and Reaction Enthalpies Calculated at CBS-QB3 Level of Theory for the Endo- and Exo-ring Closure Reactions of Scheme 6.

#	Reactants	300-2500 K			500-1500 K		298 K		E_{strain}	$\Delta_R H^{298}$	
		Modified Arrhenius Parameters			Arrhenius Parameters		Arrhenius Parameters				
		A	n	E	A''	E_a'	A'	E_a			
6.1	1,6 Endo C=CC=CCC•		2.23E+09	0.40	8.2	4.50E+10	8.7	3.18E+10	8.4	4.5	-33.9
6.2	1,7 Endo C=CC=CCCC•		1.84E+08	0.48	11.9	6.87E+09	12.4	4.63E+09	12.1	8.2	-29.5
6.3	1,6 Exo C=CC=CCC•		8.67E+09	0.47	10.1	3.06E+11	10.7	1.99E+11	10.4	2.2	-12.8
6.4	1,7 Exo C=CC=CCCC•		5.58E+08	0.55	10.4	3.54E+10	11.0	2.20E+10	10.7	2.5	-16.3




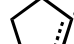






Note: ^a The units for A, A', and A'' are s⁻¹, and are kcal/mol for $\Delta_R H^{298}$, E, E_a , E_a' , and E_{strain} . ^b Molecule structures are presented in abbreviated form (H atoms missing, radical site marked with “•”) to improve readability.

Table 11: Representative Bimolecular Addition Reactions of Alkyl and Allylic Radicals to Conjugated Dienes.

Reactions	A [cm ³ /mol-s]	n	E [kcal/mol]	E _a (298 K) [kcal/mol]	Δ _r H ²⁹⁸ [kcal/mol]
Alkyl radical addition to C=CC=C					
Terminal addition					
CH ₃ + C=CC=C ↔ CCC=CC•	1.40E+05	2.3	2.6	3.9	-34.6
C ₂ H ₅ + C=CC=C ↔ CCCC=CC•	7.97E+04	2.4	2.3	3.7	-33.5
CCC• + C=CC=C ↔ CCCCC=CC•	5.40E+03	2.5	2.5	4.0	-33.1
			Average	3.9	
			STDEV	0.2	
CC•C + C=CC=C ↔ CC(C)CC=CC•	1.38E+04	2.2	1.5	2.8	-32.1
CC•C + C=C(C)C=C ↔ C=C(C)C•CC(C)C	1.50E+02	2.7	1.1	2.7	-31.6
			Average	2.7	
			STDEV	0.1	
Non-terminal addition					
CH ₃ + C=CC=C ↔ C=CC(C)C•	1.72E+05	2.3	7.2	8.6	-18.2
C ₂ H ₅ + C=CC=C ↔ C=CC(CC)C•	2.58E+03	2.6	6.2	7.8	-17.4
			Average	8.2	
			STDEV	0.6	
Stabilized radical addition to C=CC=C					
Terminal addition					
C=CC• + C=CC=C ↔ C=CCCC=CC•	4.54E+03	2.5	7.1	8.5	-18.7
C=C(C)C• + C=CC=C ↔ C=C(C)CCC=CC•	1.40E+05	2.0	6.4	7.5	-19.8
C=CC• + trans-C=CC=CC ↔ C=CCCC=CC•C	7.00E+04	2.0	7.4	8.5	-18.6
CC=CC• + C=CC=C ↔ CC=CCCC=CC•	2.60E+04	2.1	7.5	8.7	-18.5
			Average	8.3	
			STDEV	0.5	
C=CC•C + C=CC=C ↔ C=CC(C)CC=CC•	5.27E+03	2.3	6.9	8.3	-17.5
C=CC•C + trans-C=CC=CC ↔ C=CC(C)CC=CC•C	2.33E+03	2.2	6.9	8.3	-17.4
			Average	8.3	
			STDEV	0.0	
Non-terminal addition					
C=CC• + C=CC=C ↔ C=CC(C•)CC=C	1.32E+03	2.7	12.9	14.5	-1.3
CC=CC• + C=CC=C ↔ C=CC(C•)CC=CC	1.05E+03	2.6	13.0	14.5	-2.4
			Average	14.5	
			STDEV	0.0	

Note: The Arrhenius parameters are obtained in T=300-2500 K.

Table 12: Rate Constants and Reaction Enthalpies Calculated at CBS-QB3 Level of Theory for the Endo- and Exo-ring Closure Reactions of Allyl and Extended Resonance Radicals.

#	Reactants	300-2500 K			500-1500 K		298 K		E_{strain}	$\Delta_R H^{298}$
		Modified Arrhenius Parameters			Arrhenius Parameters		Arrhenius Parameters			
		A	n	E	A''	E_a'	A'	E_a		
7.1	1,3 Endo C=CC•									
		8.58E+11	0.45	51.0	2.75E+13	51.8	1.69E+13	51.3	39.9	30.3
8.1	1,5 Endo C=CC=CC•									
		7.89E+11	0.28	35.6	6.94E+12	36.1	5.11E+12	35.8	27.5	-7.5
8.2	1,5 Exo C=CC=CC•									
		9.43E+11	0.34	42.8	1.33E+13	43.4	9.19E+12	43.0	28.5	32.8
9.1	1,4 Endo C=C(C•)C=C									
		1.30E+10	0.59	38.4	1.31E+12	39.4	6.85E+11	38.7	30.4	6.9
9.2	1,4 Exo C=C(C•)C=C									
		1.19E+11	0.51	32.2	6.24E+12	33.1	3.57E+12	32.5	18.0	29.5

Note: ^a The units for A, A', and A'' are s⁻¹, and are kcal/mol for $\Delta_R H^{298}$, E, E_a , E_a' , and E_{strain} . ^b Molecule structures are presented in abbreviated form (H atoms missing, radical site marked with “•”) to improve readability.